International Journal of Steel Structures 16(4): 1009-1028 (2016)
DOI 10.1007/s13296-016-0026-7
ISSN 1598-2351 (Print)
ISSN 2093-6311 (Online)

International Journal of
STEEL
STRUCTURES
www.springer.com/journal/13296

Steel-Concrete-Steel Sandwich Composite Structures Subjected to Extreme Loads

Zhenyu Huang[1,*] and J.Y. Richard Liew[1,2]

[1]*Department of Civil and Environmental Engineering, National University of Singapore, E1A-07-03, 1 Engineering Drive 2, Singapore 117576*
[2]*College of Civil Engineering, Nanjing Tech University, Nanjing, Jiangsu 211816, China*

Abstract

This paper summarizes the latest research and development work on steel-concrete-steel (SCS) sandwich composite structures for the use as Arctic offshore platform, and to resist impact and blast loads. Current development of ultra-lightweight cement composite (ULCC) and a floatable structural cement composite (FSCC) to be used as infilled materials for SCS sandwich structure are presented. This paper aims to advance the application of SCS sandwich composite with the use of steel plate and lightweight concrete materials. A series of tests on lightweight SCS sandwich panels with shear connectors has been carried out. The superior performance of SCS sandwich panel is demonstrated. The results show that SCS sandwich with novel J-hook connectors is effective in preventing plate separation from concrete core, maintaining the structural integrity.

Keywords: Steel-concrete-steel, steel-concrete composite, sandwich structures, ultra-lightweight cement composite, blast design

1. Introduction

Steel-concrete-steel (SCS) sandwich composite structure comprises of two external steel plates with a concrete core filled in between them (Fig. 1). The composite action between the steel and concrete core is achieved by using mechanical connectors. The SCS sandwich composite exhibits significant structural and economic advantages over the conventional reinforced concrete structures in terms of higher flexural stiffness and energy absorption capacity to withstand extreme environmental and accidental loads. The external steel plates may serve as a permanent formwork during concreting, promoting construction efficiency and reducing the site handling costs and time. The waterproof feature inherently provided by external steel plates reduces surface area that needs expensive corrosive protection and makes it easy for inspection and maintenance. For conventional stiffened steel structure, plate buckling usually governed the ultimate strength so that much welding of stiffeners are needed to reduce the effective width of the plates. Large corrosion surface will be generated if using stiffened plates so that needs expensive corrosive protection. Moreover, fatigue issue becomes more pronounced issue due to much welding. Weldability issue should be addressed if high tensile strength steel and thick steel plates are used.

SCS sandwich concept reduces welding work, improve the construction efficiency and promote the structural performance which is strongly recommended to be adopted as heavy duty and protective layers such as ice-resisting walls in Arctic offshore, ship hulls, tunnels, military shelters and nuclear power station walls that require resistance against extreme loads (Huang *et al*., 2015a; 2015b; 2015c).

Weight can be reduced if using lightweight concrete so that the structure can be easier to transport and construct for Arctic offshore structures (Huang *et al*., 2015c). Curved SCS sandwich structure with slope is proposed as the ice-resisting wall to withstand the ice loading. Because sloping structures would encounter ice impact forces due to that the collided ice sheet would ride up the slope and fail in flexural bending rather than crushing as that occurred to a vertically sided structures, as shown in Fig. 2. In this way, global ice load will be alleviated. The curved geometry also helps to optimize and improve the composite action. Furthermore, modular construction with rapid installation can be achieved, reducing the fabrication cost comparing to conventional RC structures (Varma *et al*., 2015).

Received January 21, 2016; accepted May 18, 2016;
published online December 31, 2016

*Corresponding author
Tel: +65-65166498, Fax: +65-67791635
E-mail: ceehzh@nus.edu.sg

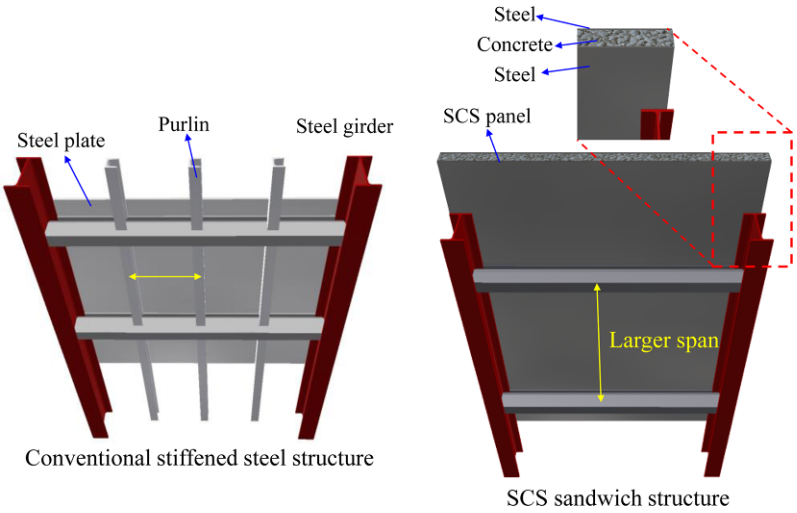

Figure 1. SCS sandwich structure v.s. conventional stiffened structure.

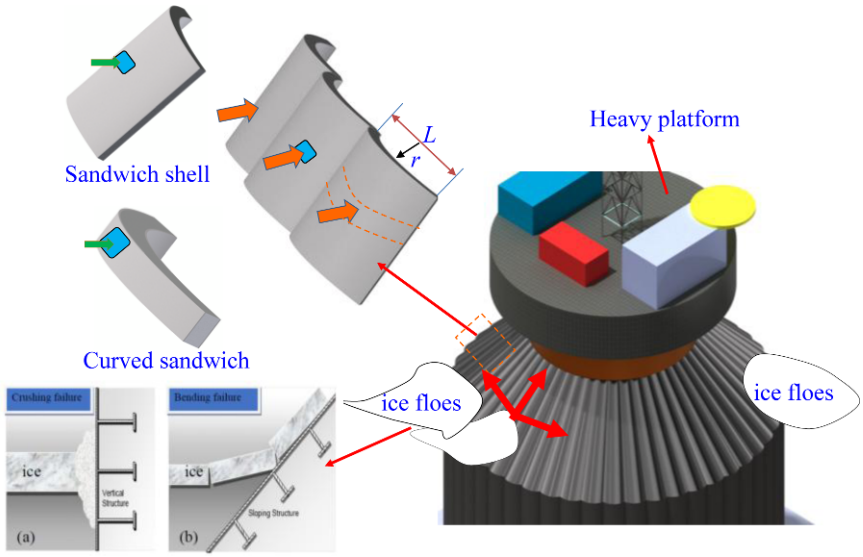

Figure 2. Gravity based Arctic offshore caisson structure using SCS sandwich.

In this paper, multiple vaults of SCS sandwich shell were designed to resist ice contact pressure. Headed shear studs or novel J-hook connectors were introduced as mechanical connectors to construct the lightweight SCS sandwich panel. This paper firstly reported the development of new lightweight cement composite materials to be used as infilled core. Mechanical properties of concretes were presented. Then, 20 curved SCS sandwich panels filled with ultra-lightweight cement composite were tested under patch load which aimed to investigate the beam-shear behaviour of curved sandwich panels. The ultimate strength behaviour of specimens were reported. Design equation was proposed to predict the shear resistances of the curved SCS sandwich panels by modifying Narayanan's equation. The accuracies of the design formulae were verified through comparing the tests results. Design recommendations were given based on the discussions and validations.

Drop weight impact tests and blast tests on SCS sandwich plates were conducted to investigate their impact and blast performance. These tests showed that J-hook shear connectors were effective in preventing tensile separation of the steel face plates, thus reducing the overall beam deflection and maintaining the structural integrity. The proposed SCS sandwich concept offered significant advantages compared with conventional stiffened steel beams and decks.

2. Development of Ultra-lightweight Cement Materials

One of the recent achievements in concrete technology is the development of ultra-lightweight cement composite (ULCC) and a floatable structural cement composite (FSCC) for marine and offshore application. The ULCC achieves

Table 1. Mix proportion and design density of ULCC

Water (kg/m^3)	OPC (kg/m^3)	SF (kg/m^3)	SRA (L)	Cenosphrere (kg/m^3)	Fiber (kg/m^3)	SP (L)	Design density (kg/m^3)
258.2	741.5	65.0	20.0	335.0	6.5	5.3	1380

*OPC: ordinary Portland cement; SF: silica fume; SRA: shrinkage reducing admixture; SP: superplasticizer

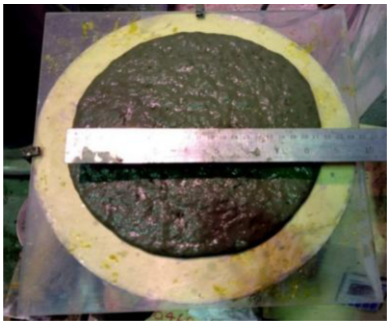

Figure 3. Flow table test of ULCC.

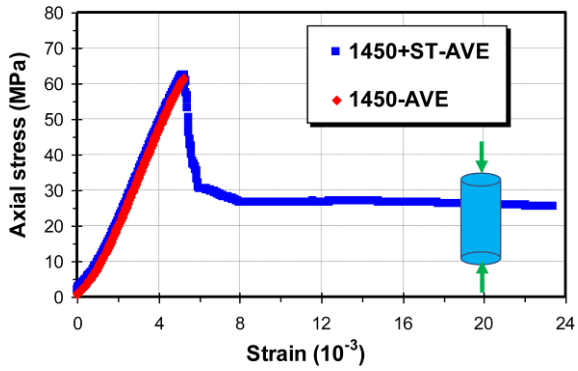

Figure 4. Compressive stress-strain curves of ULCC.

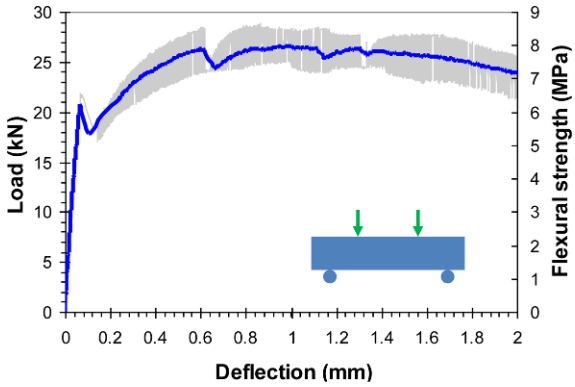

Figure 5. Flexural load-deflection curve of ULCC.

Table 2. Basic material properties of ULCC at age 28-day

Item	Material property	ULCC
1	Density after de-mould	1361 kg/m^3
2	Compressive strength cylinder f_{ck}	64 MPa
3	Ratio f_{ck} /f_{cu}	1.01
4	Splitting tensile strength	5.4 MPa
5	Flexural strength	6.7-8 MPa
6	Static modulus of elasticity	15.4 GPa
7	Static Poisson's ratio	0.25

a high compressive strengths of 60 MPa and high flexural strength of 8 MPa and hardening behaviour with only 0.5% steel fiber added (by volume) when subjected to bending tests (Wang *et al*., 2013; Huang *et al*, 2015a). ULCC is a type of novel composites characterized by combinations of low densities, high compressive strength with specific strength of up to 47 kPa/kgm^{-3}.

Table 1 shows the mix proportion and design density for ULCC. The ULCC was mixed by using a concrete pan mixer. Cylinder specimens with diameter of 100 mm and length of 200 mm were prepared to measure the compressive stress-strain curve and splitting tensile strength of ULCC at 28-day according to ASTM C39/39M (2009) and ASTM C496/C496M (2011) respectively. According to flow table test (BS EN 1015-3, 1999), around 200 mm flow is obtained shown in Fig. 3. PVA fibers with length of 6 mm and diameter of 28 μm were added at a dosage of 0.5% by volume to prevent early shrinkage and increase the ductility and tensile strength of the ULCC. Figures 4 and 5 show the typical compressive stress-strain curves and flexural load-deflection curve with hardening effect of ULCC. Table 2 shows the mechanical properties of ULCC at age 28-day.

Floating structural cement composite (FSCC) has a unit weight of less than 1,000 kg/m^3 and 28-day compressive strength of up to 30 MPa, a major breakthrough in research in cement composite materials. Figure 6 shows a floating sample of FSCC when it is placed in water. It has lower water absorptivity than that of normal weight concrete, which is essential to retain low unit weight in a marine environment. Table 3 shows the measured density after de-mould and compressive strength at age 28-day. However, so far only mechanical properties of FSCC cubs are studied and more investigations on FSCC are in process. It is expected that the use of ULCC and FSCC enables novel SCS sandwich composite structures to be developed with lower self-weight, which will provide alternatives for Arctic platform construction and ship hulls. This will benefit the transportation and installation of pre-filled structures.

3. Summary of Previous Experimental Test on Curved Sandwich Beams

3.1. Test results and discussions

The ultimate strength behaviour of curved SCS sandwich

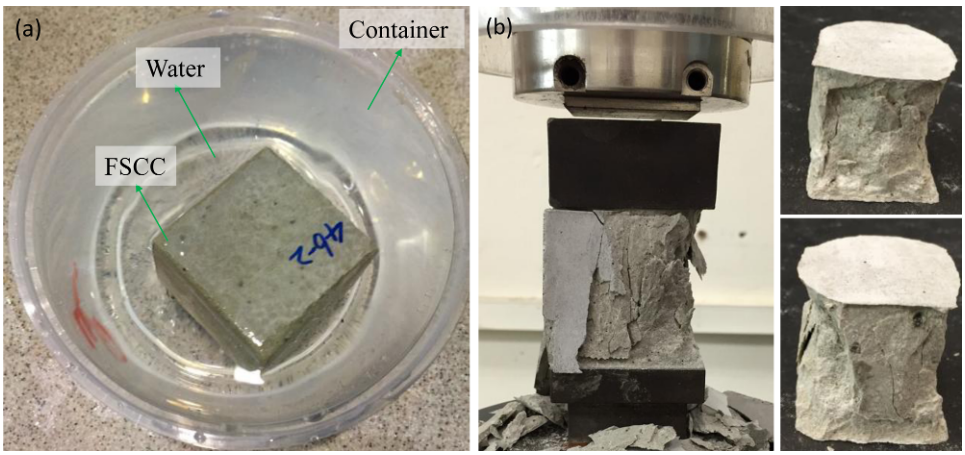

Figure 6. FSCC (a) sample in water (b) sample under compression.

Table 3. Basic material properties of FSCC at age 28-day

Item	Weight (g)	Volume (cm^3)	Density (g/cm^3)	Compressive strength (MPa)
FSCC-1	118.4	125	0.9472	29.0
FSCC-2	118.7	125	0.9496	28.1
FSCC-3	118.7	125	0.9496	29.5
FSCC-4	119.9	125	0.9592	30.3
FSCC-5	118.2	125	0.9456	31.2
FSCC-6	121.1	125	0.9688	32.3
Mean				30.0

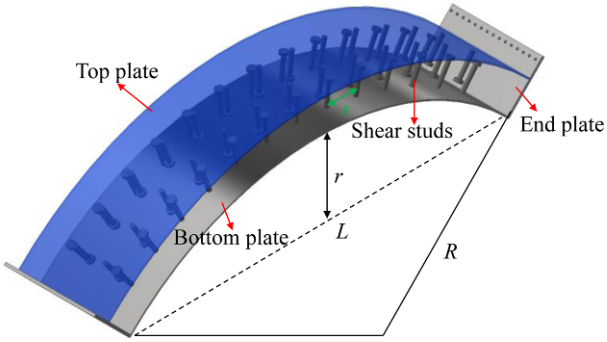

Figure 7. Typical curved sandwich beam with overlapped shear studs.

panels has been experimentally and numerically investigated (Huang *et al*., 2015a; Huang and Liew, 2015; Yan *et al*., 2015). Figure 7 shows the details of the curved sandwich panels. The test results demonstrated all the failure modes and the related load-displacement curves were captured and investigated. Parametric studies were conducted in which effect of rise-to-span ratio, span-to-thickness ratio, steel contribution ratio, degree of composite action, loading pattern and boundary conditions were considered. A unififed deep model has been developed to predict the transverse shear resistance of the flat and curved SCS sandwich panels (Huang and Liew, 2016).

3.1.1. Failure mode identification

Failure mode is the key proof to develop the ultimate strength model which can be identified by strain development, stress distribution and macroscopic collapse observations from the physical tests. The failure mode of curved SCS sandwich panels is significantly correlated to many factors, from the geometrical factors (rise-to-span ratio, span-to-thickness ratio, etc.) to loading patterns (e.g., pressure load, asymmetric pressure, punching load, load eccentricity, etc.). Geometrical conditions may change the stress flow from loading position to the part where is stiff so that leads to completely different failure mechanism. While the loading pattern may directly affect the failure path. For example, two types of ice load cases may govern the design of ice-resisting panels which are concentrated point load on a small area and lower pressure on larger area of the structure. For the former case, punching may be induced with three dimensional effects while for the latter case, flexural or shear failure (depends on the shear-span ratio) may occur with ignoring the plane strain effect. Figure 8 shows the possible failure modes of curved SCS sandwich panels.

Typically, there are seven failure modes observed from the analysis which are strongly correlated to rise-to-span ratio, steel contribution factor, span-to-core thickness ratio and loading pattern: (1) Flexural failure (Fig. 8(a)) initiates from yielding of tension plate in sandwich beam. The load-displacement curve exhibits an elastic stage and a ductile unloading behaviour. The sectional moment capacity is reached when the neutral axis moves near the lower surface of the compression steel plate (i.e. $x_c \approx 0$) until the top steel plate yields (Liew and Sohel, 2009); (2) Beam-shear mode including shear-compression (Fig. 8(b)) and shear-tension (Fig. 8(c)), is with a critical section extending in a plane across the entire width of the sandwich panels when the L/h_c ranges from 8 to 20 (Huang and Liew,

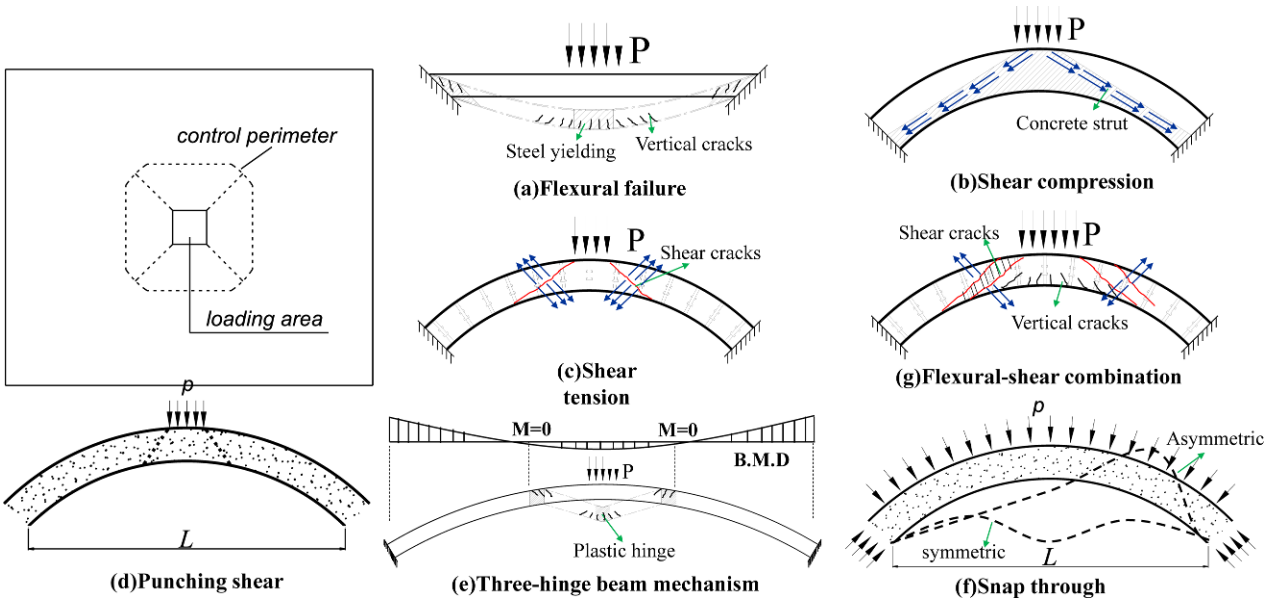

Figure 8. Possible failure modes of SCS sandwich panels.

2015). Shear-compression failure initiates inclined cracks which would propagate to the whole beam section followed by crushing of diagonal concrete strut. Therefore, the maximum resistance is governed by the concrete failure. Shear-tension failure is characterized by a major crack developed with an inclined angle. Concrete strut crushing is not pronounced and typically, the specimen fails in concrete shear and pull-out of the shear studs. So the shear resistance is governed by concrete and shear studs. The shear studs act as shear links (stirrups) to resist the diagonal shear cracks developed in concrete core; (3) Whilst, punching shear failure is with a critical section extending around the perimeter of the loaded area (Fig. 8(d)). Typically, a concrete frustum would form before the steel face plate is punched through; (4) The failure mode may change to three-hinge beam mechanism if the L/h_c is larger than 20 (Fig. 8(e)). However, the maximum pressure resistance in three-hinge beam mechanism is much lower than that subjected to other failures where the arch action is not imposed; (5) If SCS shell is subjected to uniform pressure loading, failure mode may become stability mechanisms which are symmetric and asymmetric snap-through mode (Fig. 8(f)). Other than those, with L/h_c ratio between 12.5 and 20 (e.g., L/h_c=17), mix-mode is observed (Fig. 8(g)). Asymmetric load condition causes a reduction in punching load resistance of the curved sandwich panel. It is found that the secant stiffness remains similar but the maximum resistance is lowered up to 25%, which proves that the asymmetric loading scenario is more critical and unfavorable compared to that of centrally loaded panel.

3.1.2. Benefit of using curved sandwich

Curved SCS sandwich panel can resist higher patch loads than that of a flat panel due to arching effect. Test and numerical results demonstrate that the failure mode may change to compressive related mode. Most of the part of the components are subjected to compression rather than bending so that they sustain less deflection compared to flat panels that may experience extensive deflection. This suggests that the curved sandwich panels are structurally more efficient in resisting ice pressure for Arctic offshore application. It should be noted that curved members are quite sensitive to the sliding of end supports which should be rigid design to prevent horizontal movement. This is can be guaranteed by using strong tie rods or cables to connect both end supports of curved SCS sandwich.

As a result, to improve the ultimate pressure resistance, it is recommended to utilize the arching effect. Based on the previous experimental and numerical studies (Huang *et al*., 2015a; 2015b), to achieve high resistance and ductility behaviour the optimal design parameters for the curved SCS sandwich panels subjected to patch load are summarized in Table 4.

Table 4. Optimal parameters for design of curved sandwich panels

Parameters	Recommended value
Rise-to-span ratio (r/L)	0.15~0.2
Span-to-thickness ratio (L/h_c)	8~12.5
Steel contribution ratio ($A_s f_y/A_c f_c$)	0.5-0.8
Plate slenderness ratio (s/t_s)	<27.5 (full composite)
Stud diameter-to-plate thickness (d/t_s)	<2.5 (prevent punched-through of steel plates)
End supports	Rigid joint by using tie rods or cables

3.2. Empirical model on shear resistance of curved sandwich panels

Narayanan *et al*. (1994) proposed a design method to predict the shear resistance of double skin composite beams as the following Eq. (1). However, this equation is applicable only for flat beams which ignores: (1) the effect of the rise-to-span ratio; (2) the effect of the top steel face plate and (3) overestimating the tensile resistance of the connectors embedded in concrete because the equation assumes that the shear stirrups (studs) yield all the time.

$$V=\frac{bf_{ck}h_c}{20\gamma_c}+\frac{0.5n_0A_s\sigma_u h_c}{s\gamma_a} \tag{1}$$

where f_{ck} is the compressive strength of concrete; h_c is the concrete core thickness; γ_c and γ_a are the partial safety factor for concrete and shear stud respectively (γ_c=γ_a=1.0 is used for validation); n_0 is the number of shear stud connectors behave as the transverse shear stirrups distributed in the shear failure surface; $A_s\sigma_u$ is tensile resistance of the shear stud connectors in which σ_u is ultimate strength of studs and A_s is the cross-sectional area of the studs.

A modified shear model for curved sandwich panels was suggested as,

$$V=\frac{f_{ck}}{20\gamma_c}bh_e+\sum_{i=1}^{n_{cp}}\frac{T}{s}h_c\cos\alpha_i \tag{2}$$

where, T is the tensile resistance of shear connector embedded in concrete which can be determined by Eq.(3) (Huang *et al*., 2015a); s is the connector spacing; α_i is the angle between each stud axis and vertical axis.

$$T=\min\begin{cases}T_{cb}=0.33\sqrt{f_{ck}}A_N\\ T_{pl}=0.9\varphi f_{ck}e_h d\\ T_u=\phi A_{se}f_{ut}\\ T_{ps}=A_v f_u/\sqrt{3}\end{cases} \tag{3}$$

Considering the effect of the steel face plate, the effective height of the section needs to be modified as,

$$h_e=h_c+t\frac{E_s}{E_c} \tag{4}$$

$$\alpha_i=\frac{n_i s}{R},\ (n_i=\{1,2,\ldots n_{cp}\}) \tag{5}$$

where, R is the internal radius of the arch; n_{cp} is the amount of shear studs linking the critical crack which equals to the number of shear studs welded to the bottom plate cross the crack band. Figure 9 illustrates the possible shear cracks origin from underneath the loading point to the point of inflection of the bending moment diagram in the arched member, therefore n_{cp} can be predicted by,

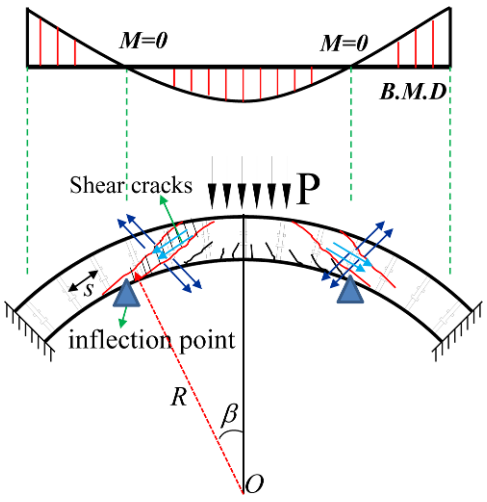

Figure 9. Possible shear cracks and inflection point.

$$n_{cp}=\text{integer}\left(\frac{b}{s}\right)\cdot\text{integer}\left(\frac{R\beta}{s}\right) \tag{6}$$

where, integer (□) represents the integer of the term in bracket; b is breadth of the member, and β represents the included angle corresponding to the inflection point of bending moment diagram.

3.3. Validation of proposed equations

All the partial safety factors in the proposed formulae are taken as 1.0 for the comparison with test results. Table 5 compares the calculated and measured shear resistance of curved sandwich panels. The predictions by Eurocode 2 method (2004), Narayanan's equation and modified Narayanan's equation are compared with 20 test results. It is found that the Eurocode 2 method and Narayanan's equation give about 33-37% over-predictions compared to the test results. The average test-to-prediction ratio is 1.37 with a coefficient of variation (COV) of 0.23 for Eurocode 2 method while these values for Narayanan's equation are 1.33 and 0.20 respectively. However, the suggested model offers the average test-to-prediction ratio of 1.08 with a COV of 0.17. Therefore, the suggested model gives a reasonable description of the shear resistance of the curved sandwich panels with acceptable accuracy. Specifically, it should be noted that the suggested method over-predicts the resistance of FSB-01 and SB-01. This is because FSB-01 fails in the flexural mode and the flexural resistance is governed by yielding of steel face plate. While for SB-01, sliding of the supports are observed during the test. The premature severe separation between bottom face plate and concrete leads to lower shear resistance. This indicates that the structural behaviour of curved sandwich panels is sensitive to the end supports which needs more investigations in the future. Therefore, FSB-01 and SB-01 are not included in the calculation of

Table 5. Comparison between calculated and tested shear resistance (curved beams)

Literature	Specimen	P_{test} (kN)	V_{test} (kN)	f_{ck} (MPa)	f_y (MPa)	s_t (mm)	h_c (mm)	V_{uEC2_m} (kN)	V_{test}/V_{uEC2_m}	V_{uN} (kN)	V_{test}/V_{uN}	$V_{u\_Eq.2}$ (kN)	$V_{test}/V_{u\_Eq.2}$
Huang *et al*., (2015)	FSB-01	132.8	66.4	58.3	397	110	100	51.6	1.29	183.2	0.36	91.9	0.72
	CSB-02	1101.3	550.7	58.3	397	110	180	349.3	1.58	329.8	1.67	432.1	1.27
	CSB-03	555.8	277.9	58.3	397	110	100	201.7	1.38	183.2	1.52	242.1	1.15
	CSB-04	452.4	226.2	41.0	397	110	100	211.4	1.07	157.3	1.44	182.1	1.24
	CSB-05	800.4	400.2	58.3	397	110	100	400.2	1.00	231.1	1.73	344.8	1.16
	CSB-06	238.6	119.3	57.39	397	110	80	92.4	1.29	107.2	1.11	121.2	0.98
	CSB-07	309.6	154.8	57.39	397	220	100	125.6	1.23	134.0	1.16	164.7	0.94
	CSB-08	458.2	229.1	57.39	397	110	100	196.3	1.17	181.8	1.26	235.5	0.97
	CSB-09	218.3	109.2	57.39	397	110	100	51.3	2.13	86.1	1.27	90.5	1.21
	CSB-10	416.4	208.2	57.39	397	110	100	195.5	1.07	181.8	1.14	234.6	0.89
Yan *et al*., (2015)	SB-01	167.9	83.9	58.00	397	145	125	132.3	0.63	154.2	0.54	185.4	0.45
	SB-02	343.5	171.7	58.00	397	145	125	155.0	1.11	154.2	1.11	195.4	0.88
	SB-03	566.1	283.1	58.00	397	145	125	172.2	1.64	154.2	1.84	199.9	1.42
	SB-04	267.1	133.5	58.00	397	145	125	134.0	1.00	154.2	0.87	187.1	0.71
	SB-05	365.9	183.0	58.00	397	145	125	131.6	1.39	154.2	1.19	184.7	0.99
	SB-06	441.6	220.8	58.00	397	228	125	134.5	1.64	137.6	1.60	187.6	1.18
	SB-07	336.6	168.3	58.00	397	342	125	110.3	1.53	128.0	1.31	163.4	1.03
	SB-08	685.2	342.6	58.00	397	145	173	176.8	1.94	211.8	1.62	255.2	1.34
	SB-09	288.0	144.0	45.00	397	145	125	115.6	1.25	129.8	1.11	148.2	0.97
	SB-10	213.9	106.9	30.00	397	145	125	88.5	1.21	101.7	1.05	98.8	1.08
	Mean value								1.37		1.33		1.08
	COV.								0.23		0.20		0.17

* $V_{uEC2\_m} = C_{lRd,c}\eta_1 k(100\rho_1 f_{lck})^{1/3} b\overline{h_c} + \sum_{i=1}^{n_{cp}} \frac{F_t}{s} h_c \cos\alpha_i$; (Narayanan *et al*., 1994);

$V_{uN} = \left(\frac{f_{ck}}{20\gamma_c} + \frac{0.5 n_0 A_s f_y}{b s_t \gamma_a}\right) b h_c$ (Narayanan et al., 1994);

$V_{u\_Eq.2} = \frac{f_{ck}}{20\gamma_c} b\overline{h_c} + \sum_{i=1}^{n_{cp}} \frac{F_t}{s} h_c \cos\alpha_i$. FSB-01 and SB-01 are not included in the calculation of the mean value and COV.

the mean value and COV in Table 5.

3.4. Finite element analysis of SCS sandwich shells

3.4.1. Material model

In numerical investigation, Concrete Damaged Plasticity (CDP) model was used to model concrete. CDP model adopted the concept of isotropic damaged elasticity in combination with isotropic tensile and compressive plasticity to represent the inelastic behaviour of concrete. The CDP model was designed for applications in which concrete was subjected to monotonic, cyclic and dynamic loading under low confining pressures and it can consider the main failure mechanisms of concrete crushing and cracking for both ABAQUS/Standard and Explicit solvers. Figure 10 shows the typical compressive and tensile model of CDP model and for simulation, the parameters are validated by the test data (Figs. 4 and 5).

For steel plates, the measured engineering stress-strain curves shown in Fig. 11 were used in FE models. The true stress-true strain relationship input in FE model can be followed by the conversion law:

$$\sigma = S(1+e) \quad (7)$$

$$\varepsilon = \ln(1+e) \quad (8)$$

where, e and S refer to the engineering strain and stress respectively obtained from standard coupon tensile tests, while σ and ε denote the true stress and true stain.

3.4.2. Element, boundary condition and contact definition

Eight node solid element with reduced integration point (C3D8R) was used to model the steel plate as well as concrete core. In this paper, full composite was defined as using perfect bond (node point coupling) between concrete and steel plate while partial composite was defined as using “hard contact” in the normal direction and “slide

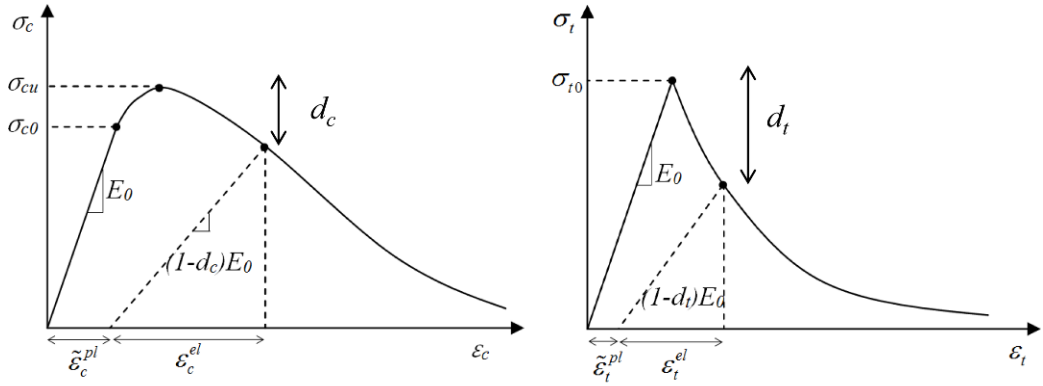

(a) Compression (b) Tensile

Figure 10. Unaxial stress-strain curve of CDP model (a) compression (b) tensile.

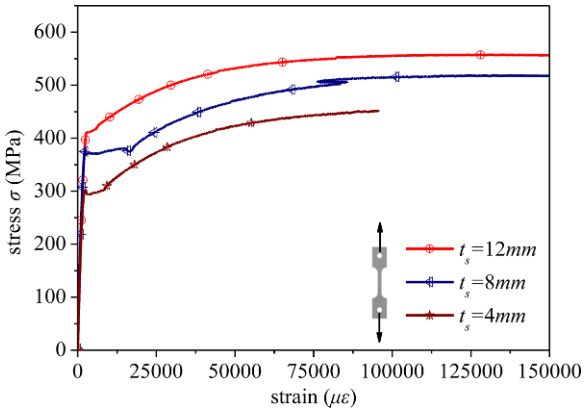

Figure 11. Stress-strain curve of steel plate.

contact" in the tangential direction. The steel plates and the concrete core interacted through the surface-to-surface "master-slave" contact interface (steel plate was the master surface). The proper contact properties were defined. A sensitivity analysis has been carried out using friction coefficient 0.2 to 0.6 and the results showed that the friction coefficient led to little difference in both overall load-deflection response and failure mode. The difference in the predicted maximum load obtained was less than 5%. Therefore, the friction coefficient value o.5 for tangential direction was used.

To verify the convergence of FE results, mesh sensitivity analysis with different mesh densities was performed before parametric study (Huang and Liew, 2015). FE model with the optimal mesh size 8-15 mm was adopted.

For curved sandwich panels, patch load was applied to the top of the specimens. Due to the symmetry in the geometry of the specimen and loading condition, one-fourth of the curved sandwich in validation phase and entire sandwich shells in parametric study were modeled, in order to improve the computational efficiency. Both ends of the curved sandwich were simulated as similar to those in the tests.

3.4.3. Verification of FE results using test data

This section compares the experimental and numerical results of load-displacement curves and failure modes of curved SCS sandwich panels. In general, FE models provided reasonable estimates of the load deflection behaviour for test specimens, including the maximum load, location of shear cracks, damaged concrete as well as the deformed shapes. In Figs. 12(a) and 13(b), the failure modes of curved SCS panels without and with connectors subjected to path loads were local snap through (SA1) and shear-tension failure (CSB-06 and CSB-07). Local buckling at free edge was observed which was also captured by FE analysis. Figures 12(b) and 13(b) compare the load-deflection curves between the test and FE results. It was found that the FE model was capable of capturing the load-deflection behaviour with reasonably good accuracy. The predicted maximum load was within 10% of the test results which indicated that the validated FE model can predict the shear behaviour well. Therefore, the proposed FE model can be used to implement the parametric studies.

3.4.4. Parametric studies and discussions

To further investigate the ultimate strength behavior of SCS sandwich shells, 12 models were created and analyzed using the validated FE model. The primary investigated parameters included rise-to-span ratio (r/L), span-to-height ratio (L/h_c), loading position, loading area and composite action. Table 6 lists the investigated parameters of SCS sandwich shell.

3.4.4.1. Effect of rise-to-span ratio (r/L)

Rise-to-span ratio affects the stiffness, failure mode and ultimate strength of SCS sandwich shell. Figure 14 shows the sandwich shells with different rise-to-span ratios (0.13, 0.21 and 0.5). From the tests, it can be found that the three SCS sandwich shells have a large concave which indicates that they fail in punching shear. The load-displacement curves with different rise-to-span ratios for partial and full composite are shown in Fig. 15(a) and

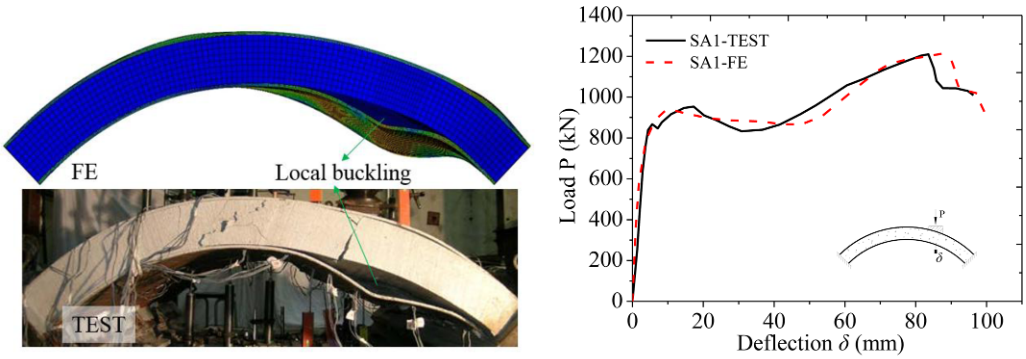

(a) Comparison of failure modes (b) Comparison of load-displacement curves

Figure 12. Experimental and numerical results of SA1.

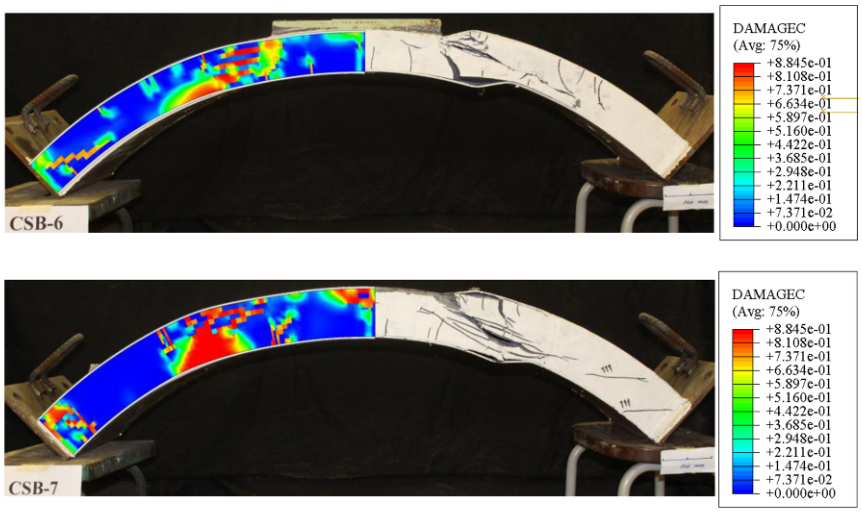

(a) Comparison of failure modes

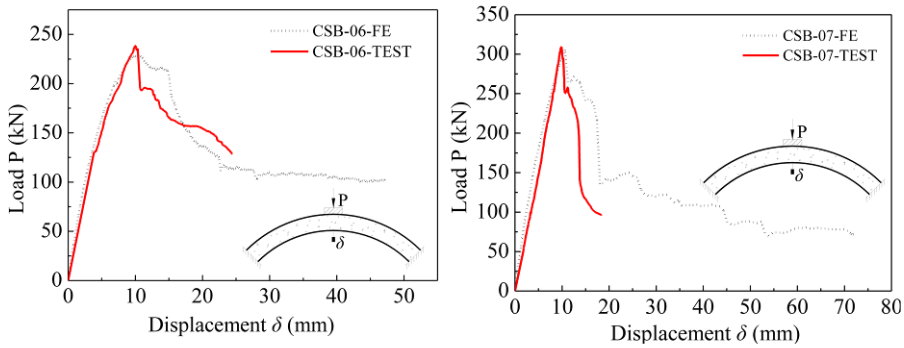

(b) Comparison of load-displacement curves

Figure 13. Experimental and numerical results of CSB-06 and CSB-07.

Table 6. Investigated parameters of SCS sandwich shell

Item	Parameters	Specification	Item	Parameters	Specification
RL013	rise/span ratio (r/L)	0.13	LP1	loading position	4-patch loading
RL021		0.21	LP2		strip pressure
RL05		0.5	LP3		half-span strip pressure
LH05	span/height ratio (L/h_c)	5	LA1	loading area	1%
LH10		10	LA2		6%
LH15		15.6	LA3		100%

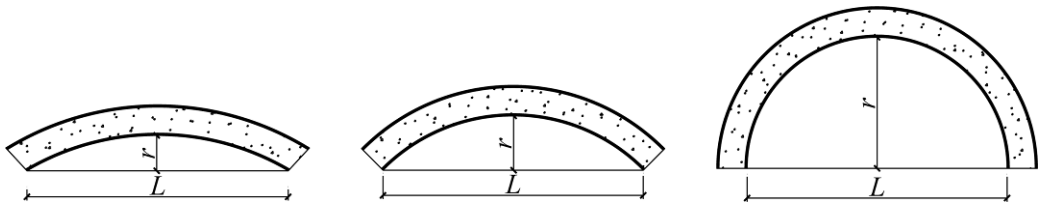

Figure 14. Curved sandwich panels with different rise-to-span ratio.

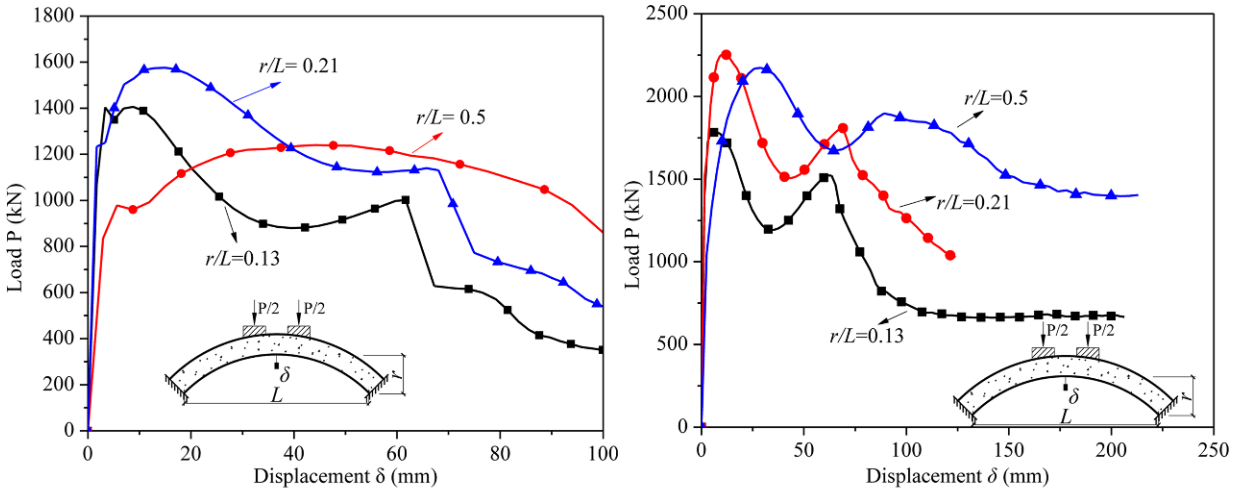

Figure 15. Load-displacement curves with varying *r/L* ratio.

15(b), respectively. Some findings can be summarized: (1) for partial composite, there are two types of load-displacement curves can be observed. The first type exhibits two peak loads among which the second peak load is smaller than the first peak value (curves of *r/L* =0.13 and 0.21) while the second type of curve exhibits a larger second peak load (curve of *r/L*=0.5); (2) for full composite, only one type of load-displacement curve is observed which is similar to the first type of curve for partial composite design. The first peak load and ultimate load of full composite sandwich shell are larger than that of partial composite design, as can be seen in Fig. 15(b); (3) it is also confirmed that SCS sandwich shell with *r/L*=0.15-0.2 behaves higher resistance and structural stiffness which is recommended for design purpose.

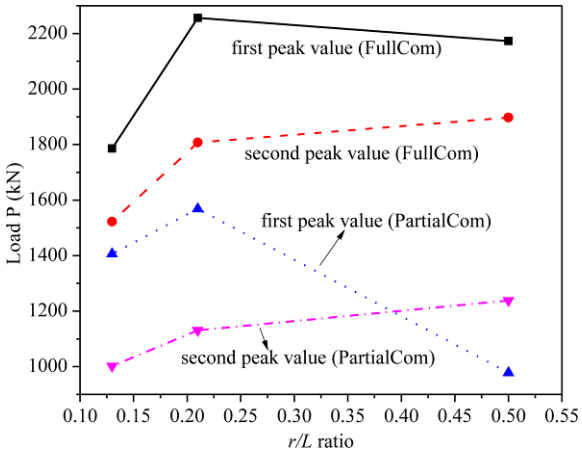

Figure 16. Effect of rise-to-span ratio on ultimate loads.

3.4.4.2. Effect of span-to-thickness ratio (L/h_c)

Span-to-height ratio also plays essential role on the resistance and ductility. With fixed *r/L* ratio of 0.13, three varying concrete core thickness h_c (*i.e.* 80, 125 and 250 mm represented the span-to-thickness ratio of 15.6, 10 and 5, respectively) were chosen to investigate the effect of span-to-thickness ratio. Deformed shapes with varying L/h_c ratio are illustrated in Fig. 17, which shows that sandwich shell with smaller L/h_c ratio would fail in punching shear (*i.e.* specimen with L/h_c=5) while for larger L/h_c ratio, combined punching and flexural is more pronounced. The comparison of load-displacement curves corresponding to different L/h_c ratios for partial and full composite are plotted in Fig. 18. Key findings are drafted as the following: (1) SCS sandwich shell with small L/h_c ratio fails in punching shear, showing the load-displacement behaviour a brittle manner with sudden punched-through of the concrete core, compared to those with larger L/h_c ratios; (2) for both partial and full composite SCS sandwich shell with L/h_c of 15.6 and 10, the load-displacement curves exhibit two peak loads. The failure mechanism corresponding to the first peak load is combined punching and flexural failure. However, the load goes up again due

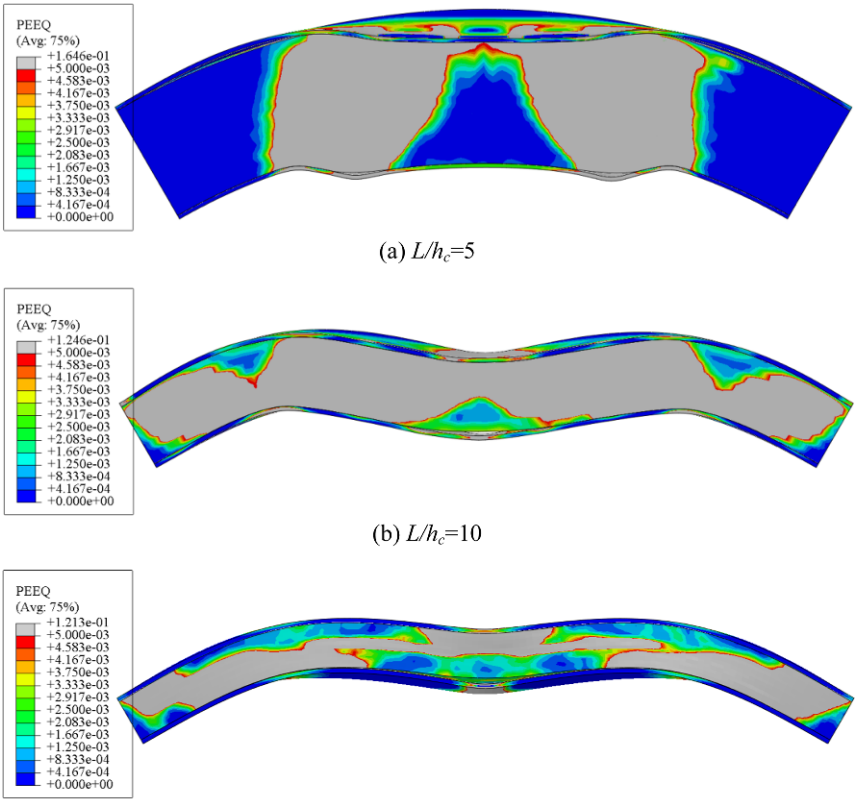

Figure 17. Deformed shapes and PEEQ distribution with varying L/h_c ratio.

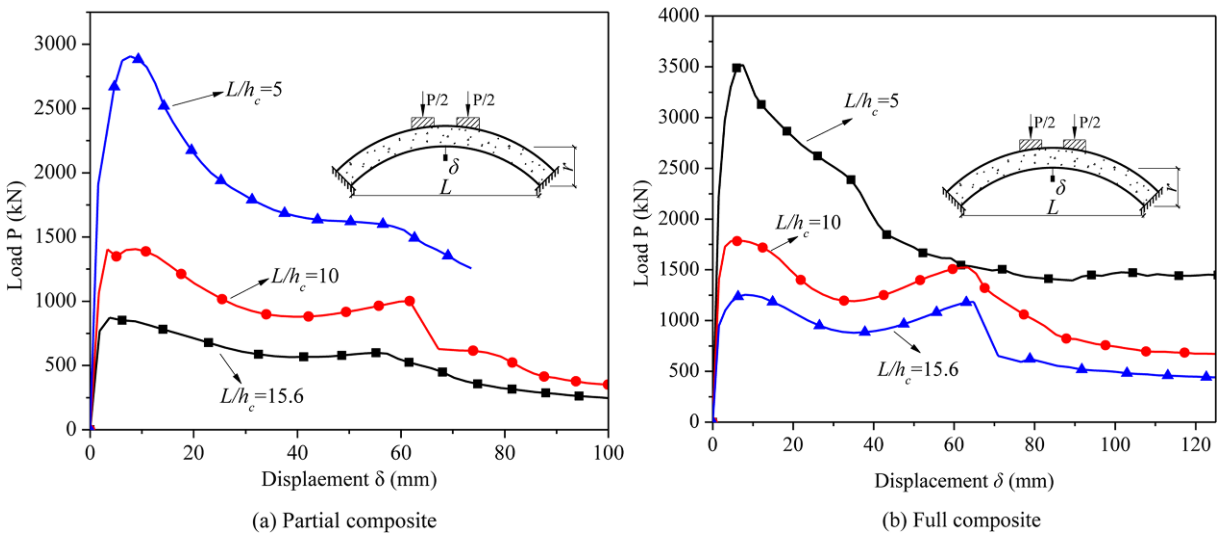

Figure 18. Load-displacement curves with varying L/h_c ratio.

to the tensile membrane effect of steel face plate after concrete failure. The tensile strain of steel face plate can achieve to yield strain at the point where the concrete core is subjected to severe damage. The second peak load cannot exceed the first peak load at the final stage. The entire structure behaves a global and ductile unloading mode; (3) for partial and full composite sandwich shell, the first peak resistance and ultimate resistance reduce as L/h_c ratio rises, as shown in Fig. 19. This indicates that the rising of L/h_c induces larger bending moment so that the failure mechanism may transform from punching mode to flexural mode.

3.4.4.3. Effect of loading area

Smaller loaded area leads to punching failure while larger loaded area makes combined failure occur prior to

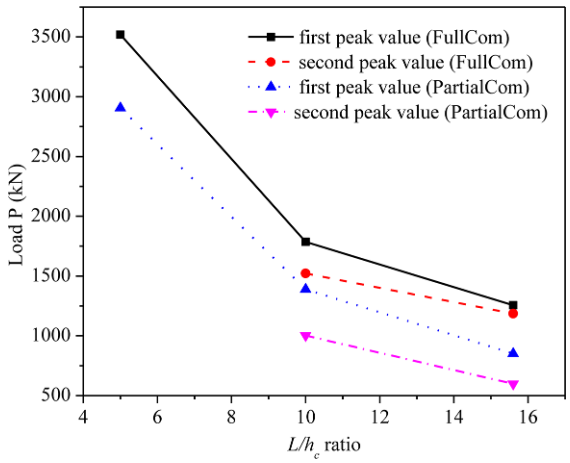

Figure 19. Effect of span-to-thickness ratio on load resistance.

punching shear. The effect of three varying loading area (1, 6, and 100% loading area) were investigated in this section. Figure 20 shows the failure modes of specimen with varying loading area applied after failure. It is found that: (1) for the case with 1% loading area applied, typical punching shear is observed. The stress distribution is concentrated around the loading area. There is basically no yielding of the bottom steel plate at any stage of loading. Failure is by punching of the concrete around the periphery of loading plate. So the resistance is mainly contributed by the concrete in punching shear; (2) for the cases with 6 and 100% loading area applied, global deformation is observed. Case (b) fails in combined punching and flexural failure while case (c) fails in symmetric snap-through mode. As can be seen in Fig. 21, the ultimate pressure resistance of the SCS sandwich shell under 4-patch loads and full-span uniform pressure are about 17.5 and 9.6 MPa, respectively. Although the pressure resistance is much lower than the punching shear resistance (52 MPa, Marshall *et al*. (2012)), it would permit large deformation and redistribution of ice pressure to the supports. In this way, much impact energy would be absorbed by the deformation of the structure.

3.4.4.4. Effect of loading position

Ice load can be from any direction toward the structure in Arctic region. Different loading patterns of pressure load in FE analysis, *i.e.* overall length and half-length of strip pressure applied on the circumferential direction of the shell, were considered. Figure 22 shows the deformed shapes of the SCS sandwich shell subjected to strip pressure loadings. Comparison of load pressure-displacement curves are shown in Fig. 21. The findings are concluded as follows: (1) generally, the failure load pressure decreases as the loading area increases and this is verified by ISO 19906; (2) failure pressure is sensitive to loading eccentricity. It is shown that the failure pressure was around 4.7 MPa for sandwich shell subjected to half-span strip pressure loading while it is around 11.6 MPa for shell subjected to full-span uniform pressure loading.

3.4.5. Comparison with design guide

Table 7 shows all the experimental and numerical data in this paper and those collected from literature. Figure 23 depicts the interaction diagrams between design ice pressure given by ISO 19906 (2010) and contact loaded area and compares with the performance of SCS sandwich shells subjected to different loading scenarios. The pressure resistance of sandwich shells obtained from experimental and numerical results are plotted in the chart, from small ice contact area (0.1 m^2) to larger contact area (32 m^2). In the chart, it is found that: (1) thin SCS sandwich cylindrical shells proposed by Shukry and Goode (1990) cannot achieve sufficient resistance to satisfy the ISO 19906 requirement when scales up to a prototype size; (2) all the sandwich shells (Huang *et al*., 2015; Yan *et al*., 2015, 2016) and full-composite SCS sandwich plates (Kumar, 2000) appear to satisfy the proposed ISO criteria. However, the partial-composite SCS sandwich plates and beams fail to sustain such applied ice contact pressure. Thus, full-composite structure is recommended for design of the SCS sandwich. To achieve full composition action, introducing mechanical shear connectors in the sandwich structures is the first choice for design purpose which plays essentially on improving the structural performances; (3) the flat panels fail in flexural mode has a lowest pressure resistance compared to that of sandwich shells fail in shear mode. This is because of the arching action which helps shell structures to enhance the resistance against the ice pressure load. The SCS shells are more superior in resisting ice contact pressure compared to flat panels.

4. Drop Weight Impact Test on SCS Sandwich Panels

Impact performance against vehicle impact and drop weight impact during lifting operations become an important concern in oil and gas production platform since impact load is a primary threat and a frequent cause of damage. Impact tests on SCS sandwich beams have been carried out to simulate the drop weight impact on SCS sandwich structure (Liew *et al*., 2009; Sohel *et al*., 2015). Ten impact tests on SCS sandwich beams were conducted. Figures 24 and 25 show the impact test set-up and failure modes of SCS sandwich beam with J-hook connector and conventional headed studs. These tests show that J-hook shear connectors are effective in preventing tensile separation of the steel face plates, thus maintaining the structural integrity and reducing the overall beam deflection. The proposed SCS sandwich concept offers significant advantages compared with conventional stiffened steel beams and decks.

Impact tests on SCS sandwich slabs were also conducted (Sohel and Liew, 2014). Based on the tests, it was found out that ULCC was superior to high strength yet brittle concrete since the core material specifically in the case

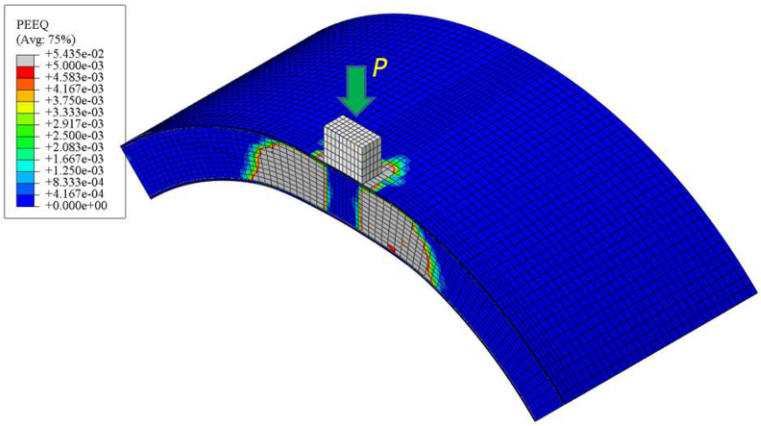

(a) 1% loading area

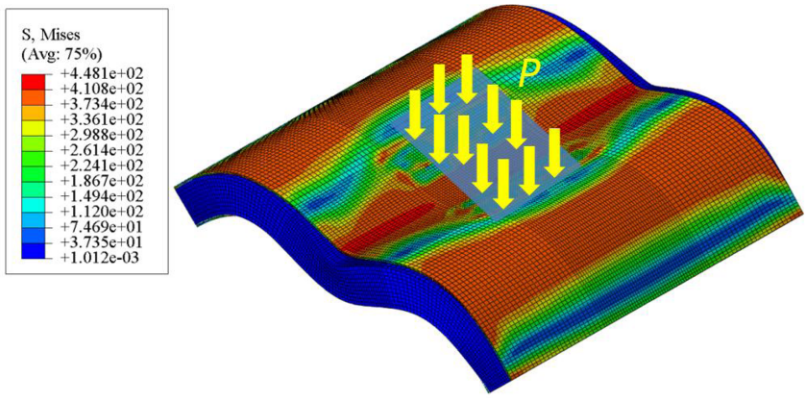

(b) 4 patch loading

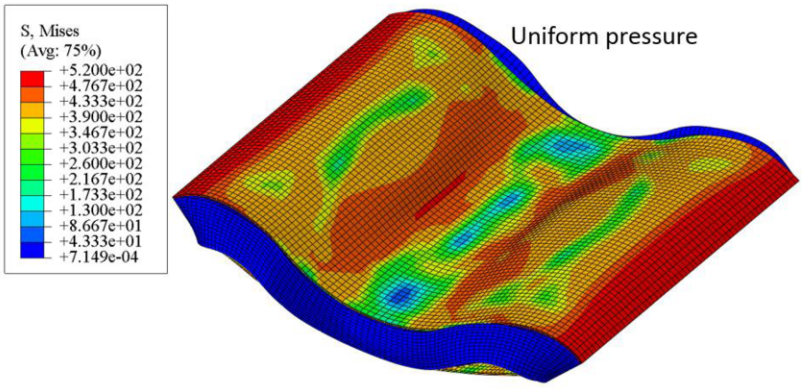

(c) 100% loading area

Figure 20. Failure modes of specimen with varying loading area.

where no shear connector was present in the composite plates. As anticipated, greater vertical displacement was noticed in plate with ULCC as the core had lower flexural rigidity. However, the top steel face plate was not punched through or even fractured when ULCC was used as opposed to the case of high strength concrete where the top steel face plate was punched through during the first impact. Secondly, steel fibers and the novel J-hook connectors were found to perform better than PVA fibers and the conventional headed shear studs respectively.

5. Blast and Ballistic Resistant Design of SCS Panels

An experimental programme was funded by Defense Agency in Singapore to investigate the resistance of SCS sandwich panels subjected to blast loads. A total of 6 specimens were fabricated for 3 blast tests (Liew and Wang, 2011; Kang *et al*., 2013). Two specimens were tested in each blast load. The configuration of the test specimens are illustrated in Fig. 26. Each specimen has a

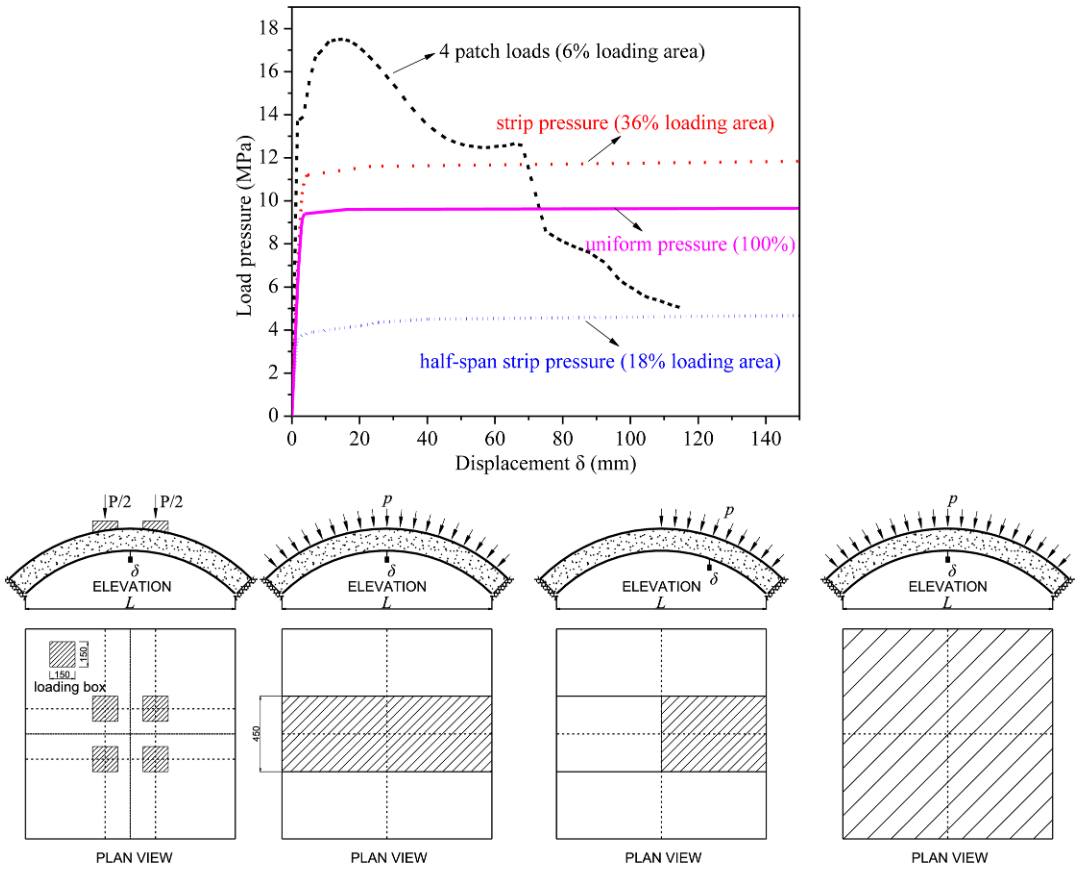

(a) 4 patch loads (b) strip pressure (c) half-span strip pressure (d) uniform pressure

Figure 21. Load pressure-displacement curves of sandwich shells subjected to different loading.

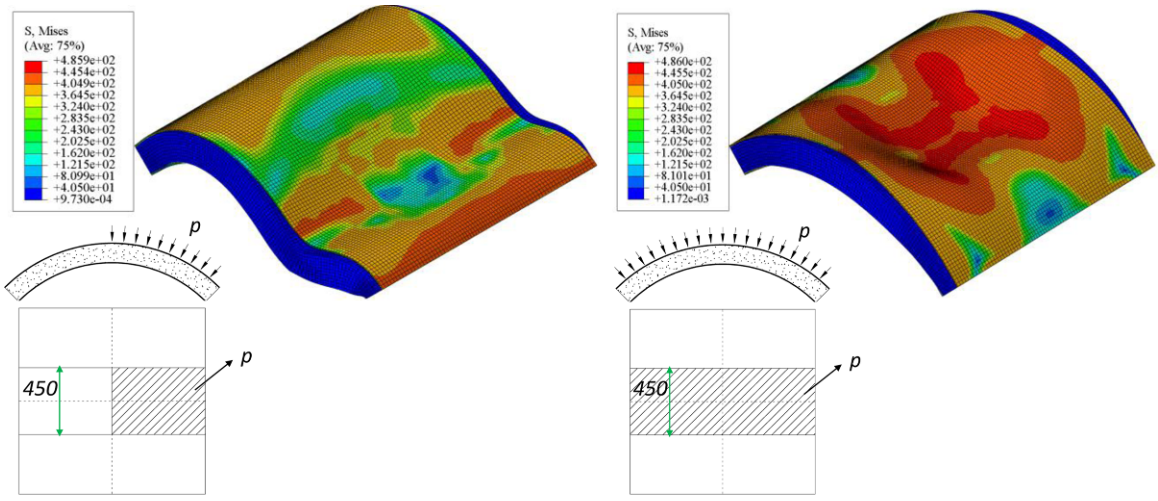

(a) half-span strip pressure (b) strip pressure

Figure 22. Failure modes of SCS sandwich shell subjected to strip pressure.

length of 1200 mm and width of 495 mm. The core thicknesses are all 70 mm. The test specimen SP was constructed as a cellular structure with internal stiffened plates welded to the steel face plates. Specimen SCS was constructed using the steel-concrete-steel sandwich concept in such a way that they have similar moment resistance and stiffness as the SP specimens.

Three different structural grade concrete materials were employed as sandwich core: normal strength concrete (NSC), lightweight aggregate concrete (LWAC) and ultra-

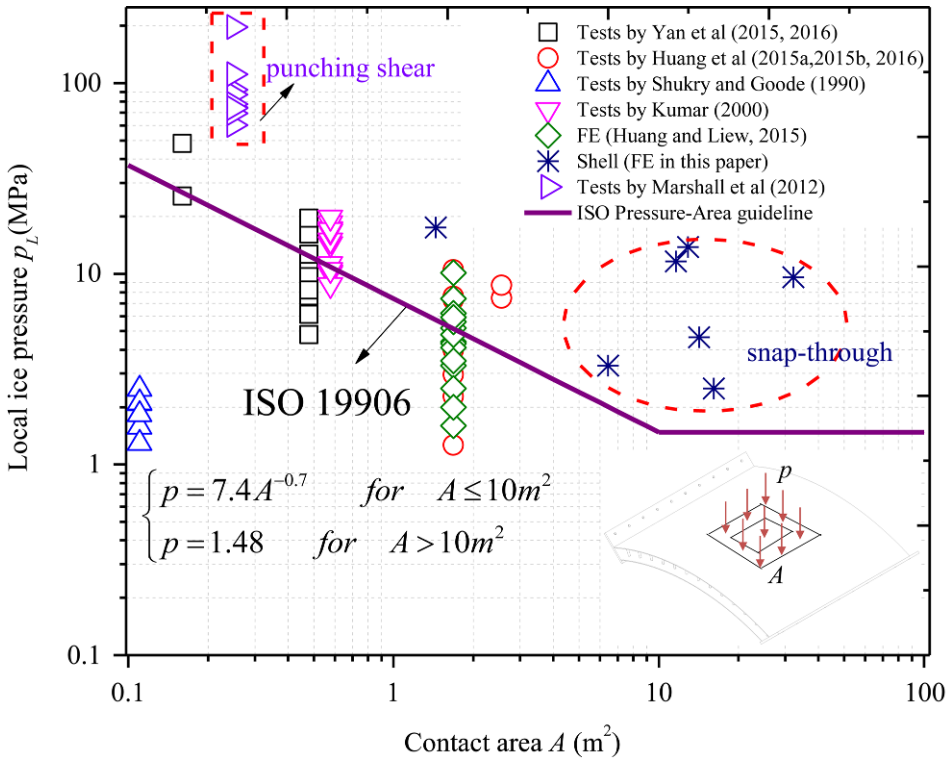

Figure 23. Resistance of experimental and numerical results V.S. design ISO 19906 ice pressure.

Table 7. Investigated parameters of SCS sandwich shell

Literature	Shell	t_s (mm)	h_c (mm)	r/L	L/h_c	connector	s (mm)	f_{ck} (MPa)	E_c (Gpa)	f_y (MPa)	f_u (MPa)	loading area (mm)	Load or pressure resistance (kN, MPa)	Failure mode
Marshall *et al.* (2012)	SA1	8.3	124.0	0.21	10.0	NILL	-	29.4	23.9	396.0	520.0	135×135	943.0	LB
	SA2	8.3	124.0	0.21	10.0	J-hook	110.0	32.6	24.0	396.0	520.0	135×135	1440.0	PS
	SA3	7.8	126.0	0.21	10.0	HSS	110.0	63.6	16.5	330.0	495.0	135×135	1363.0	PS
	SA4	7.8	132.0	0.064	10.0	HSS	110.0	72.4	16.5	330.0	495.0	135×135	1166.0	PS
	SA5	7.8	124.0	0.5	10.0	HSS	110.0	69.4	16.5	330.0	495.0	135×135	1210.0	PS
Huang *et al.* (2015)	SCSS-01	4.0	80.0	0.1	15.6	HSS	110.0	56.1	14.3	304.0	460.0	400×400	1192.9	PS
	SCSS-02	4.0	80.0	0.21	15.6	HSS	110.0	56.1	14.3	304.0	460.0	400×400	1390.9	PS
Huang and Liew (2016)	FSB-01	4.0	100.0	0.0	14.5	HSS	110.0	58.3	14.3	304.0	456.0	350×300	133.0	FF
	CSB-02	4.0	180.0	0.21	6.6	HSS	110.0	58.3	14.3	304.0	456.0	350×300	1101.0	CSC
	CSB-03	4.0	100.0	0.21	12.5	HSS	110.0	58.3	14.3	304.0	456.0	350×300	556.0	CSC
	CSB-04	8.0	100.0	0.21	12.5	HSS	110.0	41.0	14.3	371.0	480.0	350×300	452.0	SF
	CSB-05	12.0	100.0	0.21	12.5	HSS	110.0	58.3	14.3	411.0	552.0	350×300	800.0	SF
	CSB-06	4.0	80.0	0.21	15.6	HSS	110.0	57.4	14.3	304.0	456.0	350x300	239.0	SF
	CSB-07	4.0	100.0	0.21	12.5	HSS	220.0	57.4	14.3	304.0	456.0	350×300	310.0	SF
	CSB-08	4.0	100.0	0.5	12.5	HSS	110.0	57.4	14.3	304.0	456.0	350×300	458.0	SF
	CSB-09	4.0	100.0	0.21	12.5	HSS	110.0	57.4	14.3	304.0	456.0	350x300	218.0	SF
	CSB-10	4.0	100.0	0.21	12.5	HSS	110.0	57.4	14.3	304.0	456.0	350×300	416.0	SF
Yan *et al.* (2016)	P1	3.8	100.0	-	10.0	HSS	100.0	63.6	16.5	325.0	485.0	100×100	483.0	PS
	P2	3.8	100.0	-	10.0	HSS	200.0	63.6	16.5	325.0	485.0	100×100	255.0	PS

Table 7. Investigated parameters of SCS sandwich shell (continued)

Literature	Shell	t_s (mm)	h_c (mm)	r/L	L/h_c	connector	s (mm)	f_{ck} (MPa)	E_c (Gpa)	f_y (MPa)	f_u (MPa)	loading area (mm)	Load or pressure resistance (kN, MPa)	Failure mode
Yan *et al*. (2015)	BS1	4.0	130	0.21	9.6	HSS	145	57.8	17.3	301	572.0	100×100	441.6	Separation
	BS2	12.0	127	0.21	9.9	HSS	145	57.8	17.3	390	572.0	100×100	566.1	ST
	BS3	4.0	126	0.064	9.7	HSS	140	56.1	17.3	301	572.0	100×100	267.1	ST
	BS4	4.0	125.7	0.5	10.0	HSS	125	56.1	17.3	301	572.0	100×100	365.9	ST
	BS5	4.0	133	0.21	9.4	HSS	342	56.1	17.3	301	572.0	100×100	336.6	ST
	BS6	4.0	90	0.21	13.9	HSS	110	57.4	17.3	301	546.0	100×100	218.3	ST
	BS7	4.0	174	0.21	6.8	HSS	145	57.8	17.3	301	529.0	100×100	685.2	ST
	BS8	4.0	123.8	0.21	10.1	HSS	145	43.8	16.2	301	572.0	100×100	288	ST
	BS9	4.0	120	0.21	10.4	HSS	145	35	15.0	301	572.0	100×100	213.9	ST
	BS10	4.0	121.5	0.21	10.3	HSS	145	56.1	16.5	301	572.0	100×100	167.9	ST
Kumar (2000)	DSCS1	4.6	89.4	-	11.2	HSS	100.0	34.4	31.9	320.0	-	190×190	369.9	PS
	DSCS2	4.6	89.4	-	11.2	HSS	110.0	30.4	30.7	320.0	-	190×190	363.9	PS
	DSCS3	4.6	89.4	-	11.2	HSS	110.0	29.0	30.3	320.0	-	190×190	316.8	PS
	DSCS4	4.6	89.4	-	11.2	HSS	110.0	26.5	29.5	320.0	-	190×190	407.5	PS
	DSCS5	4.6	89.4	-	11.2	HSS	110.0	33.5	31.6	320.0	-	190×190	381.0	PS
	DSCS6	4.6	89.4	-	11.2	HSS	110.0	34.8	32.0	320.0	-	190×190	518.8	PS
	DSCS7	4.6	89.4	-	11.2	HSS	110.0	39.3	33.2	320.0	-	190×190	622.2	PS
	DSCS8	4.6	89.4	-	11.2	HSS	110.0	38.0	32.8	320.0	-	190×190	542.5	PS
	DSCS9	4.6	89.4	-	11.2	HSS	110.0	43.8	34.3	320.0	-	190×190	603.2	PS
	DSCS10	4.6	89.4	-	11.2	HSS	110.0	43.8	34.3	320.0	-	190×190	667.7	PS
	DSCS11	4.6	89.4	-	11.2	HSS	110.0	43.7	34.2	320.0	-	190×190	615.4	PS
	DSCS12	4.6	89.4	-	11.2	HSS	110.0	41.6	33.7	320.0	-	190×190	713.6	PS
Shukry and Goode (1990)	A1	0.97	17.6	-	-	NILL	110.0	60.5	32.2	282.0	-	83×83	14.4	PS
	A2	0.98	18.1	-	-	NILL	110.0	60.5	32.2	275.0	-	83×83	10.8	PS
	A3	1.00	17.5	-	-	NILL	110.0	60.5	32.2	274.0	-	83×83	8.9	PS
	B1	2.05	17.5	-	-	NILL	110.0	62.0	33.0	230.0	-	83×83	17.1	PS
	B2	2.03	17.3	-	-	NILL	110.0	62.0	33.0	231.0	-	83×83	14.5	PS
	B3	2.03	17.2	-	-	NILL	110.0	62.0	33.0	231.0	-	83×83	12.6	PS
	B5	1.97	18.0	-	-	NILL	110.0	63.0	35.5	249.0	-	40×40	26.4	PS
	B6	2.00	17.3	-	-	NILL	110.0	66.1	35.6	213.0	-	40×40	24.7	PS
	B7	1.97	15.8	-	-	NILL	110.0	64.6	37.1	270.0	-	40×40	21.5	PS
	C1	2.00	25.3	-	-	NILL	110.0	68.0	35.5	255.0	-	40×40	50.1	PS
	C2	1.95	25.1	-	-	NILL	110.0	66.1	35.6	266.0	-	40×40	40.2	PS
	C3	1.89	24.3	-	-	NILL	110.0	64.6	37.1	275.0	-	40×40	39.0	PS
	C4	1.94	26.1	-	-	NILL	110.0	63.0	35.5	271.0	-	40×40	32.8	PS
	D1	1.95	29.7	-	-	NILL	110.0	68.0	35.5	251.0	-	40×40	59.0	PS
	D2	1.94	30.6	-	-	NILL	110.0	63.0	35.5	276.0	-	40×40	49.0	PS
	D3	1.94	28.9	-	-	NILL	110.0	66.3	34.4	265.0	-	40×40	45.3	PS
	D4	1.93	30.8	-	-	NILL	110.0	66.3	34.4	268.0	-	40×40	43.5	PS

high strength concrete (HSC). As shown in Fig. 27, five 20 kg TNT (100 kg in total) military crater charges were arranged in an annular pattern and were placed at a standoff distance of 5 m from the specimens. The same arrangement and position of the charges were maintained in all the three blasts.

After the blast, the cellular stiffened plate panel (SP) experienced large permanent deformation (>100 mm). The SCS sandwich plate, which was subjected to the same blast load, sustained relatively less deflection. The maximum permanent mid-span deformation was 27 mm only. Considering the two specimens were designed of same face plate thickness, same stiffness and same static flexural resistance, the difference was mainly attributed to the concrete core that added mass and rigidity of the structural system. This indicates the effectiveness of SCS

Table 7. Investigated parameters of SCS sandwich shell (continued)

Literature	Shell	t_s (mm)	h_c (mm)	r/L	L/h_c	connector	s (mm)	f_{ck} (MPa)	E_c (Gpa)	f_y (MPa)	f_u (MPa)	loading area (mm)	Load or pressure resistance (kN, MPa)	Failure mode
FE results (Huang and Liew, 2015)	RL00	8.0	100.0	0	12.5	HSS	110.0	60	14.3	304	-	350×300	172	FF
	RL01	8.0	100.0	0.1	12.5	HSS	110.0	60	14.3	304	-	350×300	547	SC
	RL02	8.0	100.0	0.21	12.5	HSS	110.0	60	14.3	304	-	350×300	653	SC
	RL03	8.0	100.0	0.3	12.5	HSS	110.0	60	14.3	304	-	350×300	458	SC
	RL04	8.0	100.0	0.4	12.5	HSS	110.0	60	14.3	304	-	350×300	455	SC
	RL05	8.0	100.0	0.5	12.5	HSS	110.0	60	14.3	304	-	350×300	346	SC
	LH5	8.0	100.0	0.21	5	HSS	110.0	60	14.3	304	-	350×300	1064	CF
	LH8	8.0	100.0	0.21	8	HSS	110.0	60	14.3	304	-	350×300	774	CF
	LH12	8.0	100.0	0.21	12.5	HSS	110.0	60	14.3	304	-	350×300	653	SC
	LH17	8.0	100.0	0.21	17	HSS	110.0	60	14.3	304	-	350×300	426	THM
	LH25	8.0	100.0	0.21	25	HSS	110.0	60	14.3	304	-	350×300	261	THM
	LH40	8.0	100.0	0.21	40	HSS	110.0	60	14.3	304	-	350×300	208	THM
	FC30	8.0	100.0	0.21	12.5	HSS	110.0	30	12.1	304	-	350×300	370	SC
	FC45	8.0	100.0	0.21	12.5	HSS	110.0	45	13.5	304	-	350×300	506	SC
	FC60	8.0	100.0	0.21	12.5	HSS	110.0	60	14.3	304	-	350×300	653	SC
	FY309	8.0	100.0	0.21	12.5	HSS	110.0	60	14.3	304	-	350×300	653	SC
	FY460	8.0	100.0	0.21	12.5	HSS	110.0	60	14.3	460	-	350×300	592	SC
	FY690	8.0	100.0	0.21	12.5	HSS	110.0	60	14.3	690	-	350×300	622	SC
FE results in this paper	RL013	4.0	125.0	0.13	10.0	-	-	60.0	16.5	304.0	560.0	6.0%	1406.2	PS
	RL021	4.0	125.0	0.21	10.0	-	-	60.0	16.5	304.0	560.0	6.0%	1568.4	PS
	RL05	4.0	125.0	0.50	10.0	-	-	60.0	16.5	304.0	560.0	6.0%	978.2	PS
	LH05	4.0	250.0	5.00	6.9	-	-	60.0	16.5	304.0	560.0	6.0%	2906.4	PS
	LH10	4.0	125.0	10.00	10.0	-	-	60.0	16.5	304.0	560.0	6.0%	1388.5	Combined
	LH15	4.0	80.0	15.00	10.0	-	-	60.0	16.5	304.0	560.0	6.0%	851.5	Combined
	LP1	4.0	125.0	0.13	10.0	-	-	60.0	16.5	304.0	560.0	6.0%	1568.4	PS
	LP2	4.0	125.0	0.13	10.0	-	-	60.0	16.5	304.0	560.0	strip pressure	11.6 MPa	Snap through
	LP3	4.0	125.0	0.13	10.0	-	-	60.0	16.5	304.0	560.0	half-span strip pressure	4.7 MPa	Snap through
	LA1	4.0	125.0	0.13	10.0	-	-	60.0	16.5	304.0	560.0	1%	52.0 MPa	PS
	LA2	4.0	125.0	0.13	10.0			60.0	16.5	304.0	560.0	4%	13.8 MPa	PS
	LA3	4.0	125.0	0.13	10.0	-	-	60.0	16.5	304.0	560.0	6%	17.5 MPa	PS
	LA4	4.0	125.0	0.13	10.0	-	-	60.0	16.5	304.0	560.0	20%	3.3 MPa	Snap through
	LA5	4.0	125.0	0.13	10.0	-	-	60.0	16.5	304.0	560.0	50%	2.5 MPa	Snap through
	LA6	4.0	125.0	0.13	10.0	-	-	60.0	16.5	304.0	560.0	100%	9.6 MPa	Snap through

*LB: Local buckling; PS: Punching shear; FF: Flexural failure; CSC: Concrete strut crushing; SF: Shear failure; CF: Compression failure; THM: Three-hinge mechanism; SC: Shear compression; ST: Shear tension.

sandwich panels compared with the stiffened plate panels in terms of maintaining structural integrity and residual resistance.

SCS sandwich composite structures have been tested under both TNT detonation and ballistic tests (Fig. 28). The flexible configuration of two steel plates and concrete core made it possible for application for designing various protective structures. Through a series of tests and numerical studies carried out (Liew and Wang, 2011; Remennikov *et al*., 2012; Ma *et al*., 2013), it is demonstrated that the

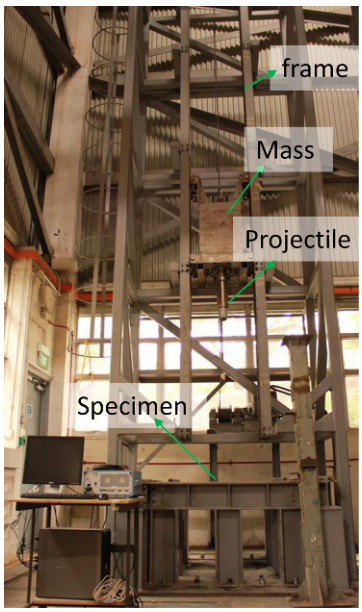

Figure 24. Drop weight impact test frame.

external steel face plate and concrete core absorbs impulse and impact energy from the blast loads, while the internal plates provide protection for the occupants.

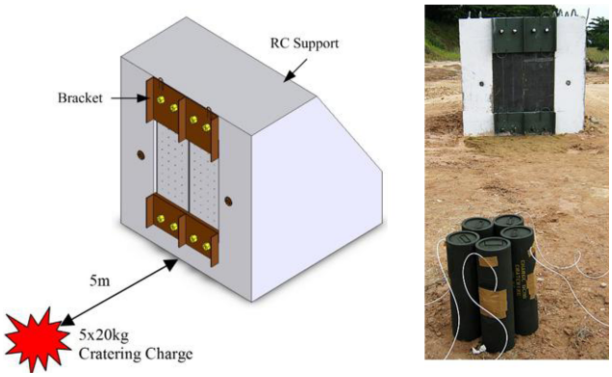

Figure 27. Blast tests: Specimen SP (left) and specimen SCSN4 (right) after blast.

Comparing with stiffened steel plate construction, the welding work and steel consumption can be reduced by using SCS sandwich concept. Due to its economical construction, SCS sandwich construction can therefore be applied in protective structures such as blast resistant building façade, blast wall construction for petrochemical industry, various blast resistant walls/doors, and ballistic resistant structures.

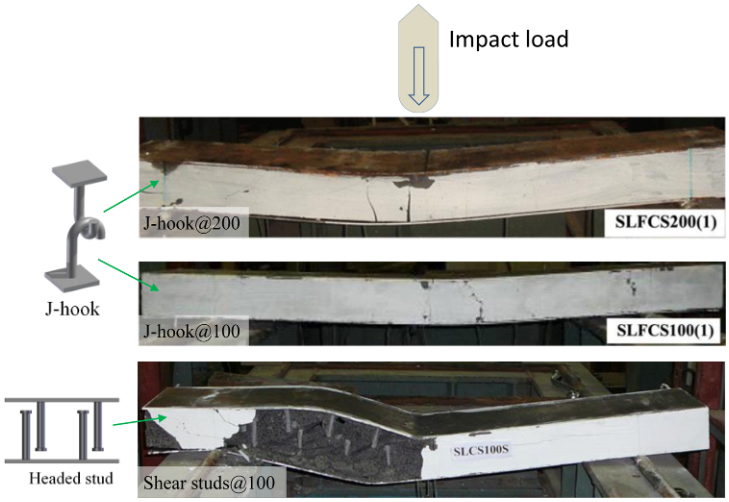

Figure 25. Damage in the sandwich beams after impact.

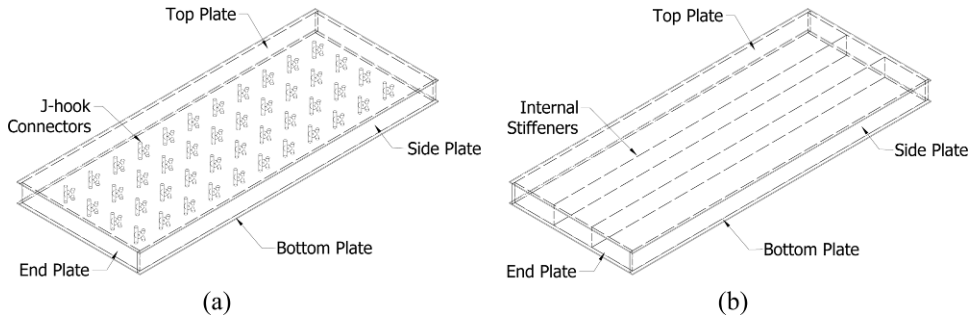

Figure 26. Configurations of (a) SCS sandwich with J-hook connectors (b) SP: cellular stiffened plate.

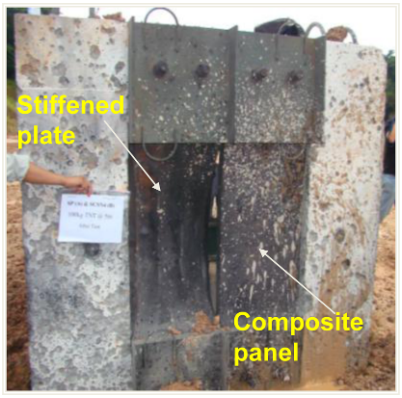

Figure 28. Comparison of stiffener plate and SCS panel subjected to TNT detonation.

6. Conclusions

This paper summarizes the developments of the novel Steel-Concrete-Steel (SCS) sandwich structures in the structural laboratory at the National University of Singapore. Lightweight and high strength cement composite (ULCC and FSCC with density ranged from 980-1500 kg/m^3 and compressive strength ranged from 30-60 MPa) and novel J-hook connectors are developed for the use of SCS sandwich structure. Steel-concrete-steel sandwich panel filled with ultra-lightweight cement composite is proposed for Arctic oil/gas production platform to sustain the extreme loads such as quasi-static ice impact pressure, drop weight impact, vehicle impact and blast loads. The panels can be constructed onshore benefiting from lower costs, existing construction yards, and the ability to construct all year round. The space between the two shells can then be filled with ultra-lightweight high strength cement composite. This will benefit the transportation and installation of pre-filled structures in the Arctic region. These development works are necessary to form a robust and safe structure which is strong enough to resist these extreme forces. Experimental and analytical studies are carried out to investigate the structural behaviours of the SCS sandwich structures under quasi-static, impact and blast loads. Based on these experimental and analytical studies, the following conclusions can be drawn:

(1) Designed in same resistance, SCS sandwich structures can reduce the self-weight and increase the strength-to-weight ratio of the structure compared with that using normal stiffened plate structures.

(2) Empirical formulae, *i.e.*, Eqs. (2)-(6), have been proposed to predict the shear resistance of the curved SCS sandwich panels. Through the validations against 20 tests on sandwich panels, the predictions by the empirical formulae exhibite close correlations to the test results.

(3) A nonlinear 3D finite element model is developed to investigate the behaviour of SCS sandwich composite panels infilled with ultra-lightweight cement composite. The FE model is validated against the experimental results from the published literatures. Parametric studies show that both geometrical conditions (i.e., rise-to-span ratio, span-to-thickness ratio) and loading patterns (i.e., loading area and loading position) are all strongly correlated to the ultimate strength of SCS sandwich shells. Because of the arching action, the SCS sandwich shells can resist higher contact pressure than that of a flat panel but this is valid only if the end supports are restricted.

(4) This paper supplements the limited test data on the SCS sandwich structures under larger ice-contact area by FE analyses, and the results show that full composite SCS sandwich shells fail in snap-through mode, combined punching and flexural mode all satisfy the proposed ISO criteria which indicates that they are suitable for engineering application in the Arctic region.

(5) A series of tests on SCS sandwich beams and slabs subjected to drop weight impact loads is carried out to investigate the structural performance of the SCS sandwich structures and the test results demonstrate the effectiveness of novel J-hook shear connectors in preventing separation between steel face plates and concrete core and the superior structural integrity performance of the SCS sandwich system.

(6) Large scale tests on the SCS sandwich panels subjected to blast load are carried out. The blast performance of the SCS sandwich panels improves with the increase in the flexural and shear stiffness and the weight of the internal core material. Tests on SCS sandwich panels demonstrate promising structural performance, engineering flexibility and construction economy making them suitable for the use as protective structures.

(7) So far for design purpose, the ultimate resistance of SCS sandwich segments are evaluated, and further studies should extend to global performance of ice-resisting cone structure using SCS sandwich subjected to ice load. In this case, the joints connecting to the different sandwich composite panels becomes more essential that need more investigations.

Acknowledgments

The authors would like to acknowledge the research grant R-302-501-002-490 received from the Maritime and Port Authority (MPA) of Singapore for conducting parts of the works reported herein. The part of research work done by Dr KMA Sohel, Dr Kang KW are gratefully acknowledged.

References

ASTM C39/C39M-09. “Standard Test Method for Compressive Strength of Cylindrical Concrete Specimens”.

ASTM C496/C496M-11. “Standard Test Method for Splitting Tensile Strength of Cylindrical Concrete Specimens”.

BS EN 1015-3-1999. “Methods of Test for Mortar for Masonry”.

BS EN ISO 19906 (2010). "Petroleum and Natural Gas Industries-Arctic Offshore Structures", BSI Standards Publication.

Euro Code 2 (2004). "Design of concrete structures-Part 1-1: General rules and rules for buildings". BS EN 1992-1-1.

Huang, Z.Y., Liew, J.Y.R., Xiong, M.X. and Wang, J.Y. (2015a). "Structural behaviour of double skin composite system using ultra-lightweight cement composite." *Construction and Building Materials*, 86, pp. 51-63.

Huang, Z.Y., Wang, J.Y., Liew, J.Y.R., Marshall, P.W. (2015b). "Lightweight steel-concrete-steel sandwich composite shell subject to punching shear. *Ocean Engineering*, 102, pp. 146-161.

Huang, Z.Y., Palmer, A.C., Marshall, P.W, Liew, J.Y. R (2015c). "Arctic platform constructions using steel-concrete-steel sandwich composite, *23th International Conference on Port and Ocean Engineering under Arctic Condition (POAC)*, NTNU, Trondheim, Norway, June 14-18, 2015.

Huang, Z.Y, Liew, J.Y.R. (2015). "Nonlinear finite element modelling and parametric study of curved steel-concrete-steel double skin composite panel filled with ultra-lightweight cement composite". *Construction and Building Materials* 2015; 95, pp. 922-938.

Huang, Z.Y., Liew, J.Y.R. (2016). "Experimental and analytical studies of curved steel-concrete-steel sandwich panels under patch loads". *Materials & Design*, 93, pp. 104-117.

Kang, K.W., Lee, S.C., Liew, J.Y.R. (2013). "Analysis of steel-concrete composite column subject to blast". *Structures and buildings*. 166(SB1), pp. 15-27.

Kumar, G., "Double skin composite construction". M. Eng. Thesis National University of Singapore, Singapore, 2000.

Liew, J.Y.R., Sohel, K.M.A. (2009). "Lightweight steel-concrete-steel sandwich system with J-hook connectors". *Engineering Structures* 31, pp. 1166-1178.

Liew, J.Y.R., Sohel, K.M.A., Koh, C.G. (2009). "Impact tests on steel-concrete-steel sandwich beams with lightweight concrete core", *Engineering Structures* 31(9), pp. 2045-2059.

Liew, J.Y.R., Wang, T.Y. (2011) "Novel Steel- Concrete-Steel Sandwich Composite Plates Subject to Impact and Blast Load" *Advances in Structural Engineering*, 14(4), pp. 673-688.

Marshall, P., Sohel, K., Liew, R.J., Yan, M., Palmer, A.C. and Choo, Y.S. (2012). "Development of SCS composite shell for Arctic caissons." *Proceedings, Arctic Technology Conference*, Houston, paper OTC23818.

MA, C.Y., and Liew, J.Y.R. (2013). "Blast and Ballistic Resistance of Ultra-High Strength Steel". *Journal of Protective Structures*, 4(3), pp. 379-413.

Narayanan, R., Roberts, T.M., Naji, F.J. (1994). "Design guide for steel-concrete-steel sandwich construction, Volume 1: General principles and rules for basic elements", The Steel Construction Institute, Ascot, Berkshire, UK.

Remennikov, A.M., Kong, S.Y. (2012). "Numerical simulation and validation of impact response of axially-restrained steel-concrete-steel sandwich panels". *Composite Structures*, 94, pp. 3546-3555.

Shukry, M.E.S., Goode, C.D. (1990). "Punching shear strength of composite construction". *ACI Structural Journal*. 87(1) , pp. 12-22.

Sohel, K.M.A., Liew, J.Y.R. (2014). "Behavior of steel-concrete-steel sandwich slabs subject to impact load". *Journal of Constructional Steel Research* 100, pp. 163-175.

Sohel, K.M.A., Liew, J.Y.R, Koh, C.G. (2015). "Numerical modelling of lightweight Steel-Concrete-Steel sandwich composite beams subjected to impact." *Thin-Walled Structures*, 94, pp. 135-146.

Varma, A.H., Malushte, S.R., Lai, Z.C. (2015). "Modularity & innovation using steel-plate composite (SC) walls for nuclear and commercial construction", *11th International Conference: Advances in Steel-Concrete Composite Structures (ASCCS)*, Beijing, China, Dec 3-5, 2015.

Wang, J.Y., Chia, K.S., Liew, J.Y.R, Zhang, M.H. (2013). "Flexural performance of fiber-reinforced ultra-lightweight cement composites with low fiber content". *Cement Concrete Composite*, 43, pp. 39-47.

Yan, J.B., Liew, J.Y.R, Qian, X.D., Wang, J.Y. (2015) "Ultimate strength behavior of curved steel-concrete-steel sandwich composite beams". *Journal of Constructional Steel Research*; 115, pp. 316-328.

Yan, J.B., Liu, X.M., Liew, J.Y.R., Qian, X.D., Zhang, M.H. (2016). "Steel-concrete-steel sandwich system in Arctic offshore structure: Materials, experiments, and design". *Materials & Design* 91, pp. 111-121.